Front. Chem. Sci. Eng. 2022, 16(1): 92–102
https://doi.org/10.1007/s11705-021-2063-9

RESEARCH ARTICLE

In-situ hydrophobic environment triggering reactive fluorescence probe to real-time monitor mitochondrial DNA damage

Beidou Feng, Huiyu Niu, Hongchen Zhai, Congcong Shen, Hua Zhang (✉)

School of Chemistry and Chemical Engineering, Henan Normal University, Xinxiang 453007, China

Abstract Mitochondrial DNA has a special structure that is prone to damage resulting in many serious diseases, such as genetic diseases and cancers. Therefore, the rapid and specific monitoring of mitochondrial DNA damage is urgently needed for biological recognition. Herein, we constructed an *in situ* hydrophobic environment-triggering reactive fluorescence probe named MBI-CN. The fluorophore was 2-styrene-1*H*-benzo[*d*]imidazole, and malononitrile was introduced as a core into a molecule to initiate the hydrolysis reaction in the specific environment containing damaged mitochondrial DNA. In this design, MBI-CN conjugates to mitochondrial DNA without causing additional damages. Thus, MBI-CN can be hydrolyzed to generate MBI-CHO in an *in situ* hydrophobic environment with mitochondrial DNA damage. Meanwhile, MBI-CHO immediately emitted a significative fluorescence signal changes at 437 and 553 nm within 25 s for the damaged mitochondria DNA. Give that the specific and rapid response of MBI-CN does not cause additional damages to mitochondrial DNA, it is a potentially effective detection tool for the real-time monitoring of mitochondrial DNA damage during cell apoptosis and initial assessment of cell apoptosis.

Keywords hydrolysis reaction, mitochondrial DNA damage, *in situ* hydrophobic environment trigger, fluorescence probe, apoptosis

1 Introduction

Mitochondrial DNA (mtDNA) is a special nucleic acid molecules associated with special physiological actions, such as matrilineal inheritance [1,2]. Owing to its special circular structure, mtDMA is vulnerable to damage due to external environments (such as ultraviolet light and radiation) and the internal factors of the organism (such as copy errors, oxidative deamination, and reactive oxygen species). When mtDNA is damaged, its structural unwinding would be caused by a mass of damage, which will cause changes in the surrounding microenvironment. These damages further accelerate the unwinding of mtDNA [3,4]. Furthermore, due to not the protection of the histone and other DNA binding protein, it cannot be repaired once the damage occurs [3–8]. In addition, changes in the surrounding microenvironment are complex and rapidly fluctuate. Moreover, if not repaired in time, mtDNA damage and the corresponding environmental changes causes cell cycle arrest, senescence, or programmed cell death, which poses a threat to the organism and even lead to the occurrence of serious physical diseases [2,4,7–19] and mitochondrial dysfunction, genome destruction, and hereditary diseases [2,9–20]. Therefore, a method that can quickly and specifically monitor mtDNA damage and corresponding environmental changes in organisms should be developed.

To date, many fluorescent probes based on rhodamine, cyanine, boron-dipyrromethene, anthraquinone, 1,8-naphthalimide and metal complexes have been fabricated for DNA detection [19,21–30]. Although these probes facilitates the visualization of cell DNA, they have some shortcomings, such as slow response [22], poor specificity [23,26], extra damage [24–27], and so on, which hinder their wide application. For example, Zou et al. [22] designed a SG-RB probe using cationic rhodamine entity as the mitochondrial targeting group. SG-RB can selectively bind to mtDNA and produces green fluorescence in the mitochondria of living cells. However, towing to its long binding time to mtDNA, the *in situ* monitoring of rapid changes due to mtDNA damage is difficult. Abeywickrama et al. [23] reported a case of near-infrared

Received December 29, 2020; accepted March 24, 2021

E-mail: zhanghua1106@163.com

red cyanine probe, which possesses large stoke shift and is highly selective toward DNA. However, cell imaging experiments show that this probe cannot respond to mtDNA. The anthraquinone dye DRAQ5 emits red fluorescence and specifically labels DNA, but it damages the DNA structure [27]. Hence, probes that can quickly and specifically recognize mtDNA damage and corresponding environmental changes without causing additional damage to mtDNA are urgently needed.

Herein, based on microenvironmental changes initiated by hydrolysis reaction, a MBI-CN probe was designed and synthesized for the rapid and specific real-time monitoring and evaluation of mtDNA damage. A typical dye molecule, 2-styrene-1*H*-benzo[*d*]imidazole (MBI), was selected as the fluorophore because it can easily embed mtDNA double strand and effectively prevent additional damage to mtDNA [10,28,29]. The hydrolysis reaction of the malononitrile group in a hydrophobic environment was selected as the identification reaction [10,31–35]. Malononitrile was introduced into this probe. When the mtDNA is damaged, microenvironment changes occur, and malononitrile in MBI-CN is hydrolyzed [10,31,36,37]. The generated aldehyde-based molecule MBI-CHO can cause changes in the fluorescence signal of mtDNA damage and can thus facilitate the rapid and specific monitoring of mtDNA damage. The identification reaction can be activated by microenvironment changes during mtDNA damage, and different fluorescence signals emitted. On the basis of these changes, it facilitates the quick and specific monitoring of small mtDNA damage and provides early warning information for the occurrence of diseases.

2 Experimental

2.1 Materials and instrumentation

All reagents and solvents were obtained from commercial suppliers and were used without further purification. All solvents used in spectrum test systems were chromatographically pure. DNA digestive enzymes were purchased from TIANGEN RNase-free DNase I. Column chromatography (silica gel powder, 200–300 mesh) was used in the separation and purification of compounds. ^{1}H NMR and ^{13}C NMR were performed using an AVANCE III HD 600 MHZ spectrometer (Bruker Co. Switzerland). High-resolution mass spectrometry was measured with an ultrahigh-resolution electrospray time-of-flight mass spectrometry system (Bruker Co. Switzerland). The circular dichroism was performed using circular dichroism spectrometers. Absorption and emission spectra were collected using a Cintra 2020 spectrophotometer (GBC Australia) and FluoroMax-Plus spectrophotometer (HORIBA Japan). Cell imaging was performed using an Olympus spectroscopy confocal multiphoton microscope (FV1200) and MaiTai femtosecond laser light source (specr-physics).

2.2 General procedure for the spectra measurement

The tested probe molecules were prepared in dimethyl sulfoxide solvent as a stock solution (6.0 mmol). The test was performed by placing 1.0 μL of the probe stock solution and 3.0 mL of the test solvent in a 3.0 mL cuvette and mixing them thoroughly. Each test experiment was repeated five times ($n = 5$). The excitation wavelength used in the test was the maximum absorption wavelength of the molecule.

An mtDNA solution was prepared, and the concentration was messured with an ultraviolet spectrophotometer. Give that pure mtDNA has a strong absorption peak at 260 nm, mtDNA can be quantified by determining the absorption peak at 260 nm. A certain amount of mtDNA was added to high-purity water, and the solution was mixed upside-down. Approximately 10 μL of mtDNA solution was added to 3 mL of high-purity water in a dilution ratio of 1:300 dilution. Then, ultraviolet absorption value was recorded at 260 nm, and the concentration of mtDNA was calculated as follows: C_{mtDNA} ($\mu g \cdot mL^{-1}$) = 50 × (OD_{260nm}) × dilution times.

2.3 Molecular docking calculation

Molecular docking was performed using a Yin Fo Cloud computing platform for the calculation of the docking mode between the molecules and mtDNA. The docking mode of protein/nucleic acid/polypeptide/small molecule docking was adopted. DOCK 6.9 was used, and the docking method of lock-and-key was adopted for flexible ligand docking.

2.4 Circular dichroism spectrum determination

Circular dichroism is a powerful tool for studying the interaction between mtDNA and small molecules. The circular dichroism spectrum is extremely sensitive to conformational changes in mtDNA, especially within a range of 180–320 nm [38]. The circular dichroism of mtDNA is produced by asymmetric sugar molecules in its backbone structure, and the helical structure is determined according to the configurations of the sugar molecules. When the small molecule mtDNA acts, it affects the original mtDNA circular dichroism signal. On the basis of signal changes, the interaction between small molecules and mtDNA can be determined, and the different modes of binding between the small molecules and mtDNA can be inferred [39]. During the circular dichroism spectrum test, Tris-HCl (0.05 mol, pH = 7.4) was used as the solvent for determination. Different concentrations of molecular probes (0–0.75 mmol) were added to the mtDNA (0.25 $mg \cdot mL^{-1}$) solution for the recording of the spectra of each sample at 205–370 nm.

2.5 Cytotoxicity assays

Cytotoxicity tests were performed in 96-well plates. HepG 2 and 3T3 cells were spread on 96-well plates at a density of 5×10^4 cells per well, and the incubation time was 24 h. Different concentrations (5.0, 10.0, and 15.0 $\mu mol \cdot L^{-1}$) of the probes (MBI-CHO and MBI-CN) were added to the wells. After incubation for 24 h, 20 μL of 3-(4,5-dimethyl-2-thiazolyl)-2,5-diphenyl-2-*H*-tetrazolium bromide (MTT) solution (5.0 $mg \cdot mL^{-1}$) was added to each well. Finally, cytotoxicity data were collected and processed with an enzyme marker.

2.6 Cell culture and fluorescence imaging

HepG 2 and 3T3 cells were cultured in Dulbecco's Modified Eagle Medium (Corning) containing 10% fetal bovine serum (Sigma Aldrich) and 1% penicillin/streptomycin (Corning). Cell culture conditions were 37 ºC and 5% CO_2. A day before imaging, the cells were spread on a cell culture dish at a density of 20000 cells per milliliter. After 24 h of incubation, MBI-CN and commercial mitochondrial green dye were added, and imaging was performed after 30 min of incubation. The laser excitation wavelengths were 405 and 488 nm, and the fluorescence collection ranges were 495–535 and 580–620 nm.

2.7 Intracellular DNA digestion experiment and cell imaging

HepG 2 cells were used as research objects. Before imaging, the cells were plated in a cell culture dish and cultured for 24 h, then washed with cold methanol four or five times. Approximately 2.0 mL of ice methanol was added, and the cells were incubated at 4 °C for 30 min. The cells were washed with phosphate buffer saline before 2.0 mL of phosphate buffer saline was added and incubated with DNase I digestion enzyme for 2.0 h at 37 °C and 5% CO_2. The cells were incubated with the probes 30 min, then observed under a fluorescence microscope. The laser excitation wavelength was 405 nm, and the fluorescence collection ranges were 415–465 and 530–570 nm.

3 Results and discussion

3.1 Molecular design and synthesis

For the development fluorescent probes that can used in quickly and specifically monitoring mtDNA damage in living organisms, Knoevenagel condensation of 2-methylbenzimidazole and terephthalaldehyde (Scheme 1) was carried out to extend its conjugate system. The connection formed a typical chromophore with a twisted intramolecular charge transfer system. Benzo[*d*]imidazole was introduced to MBI-CN and its product, MBI-CHO, to specific targeting of mtDNA, given that this group can specifically bind to mtDNA and effectively prevent additional damage to mtDNA [32]. The hydrolytic rate-limiting reaction of malononitrile was selected as the specific recognition reaction because it can be triggered by the intracellular microenvironment changes caused by mtDNA damage and unwinding [10,31–35]. Therefore, malononitrile was introduced into the probe for the synthesis the fluorescent probe MBI-CN, which not only can be used in detecting microenvironmental changes caused by mtDNA damage but also can be used in quickly and accurately monitoring and evaluating mtDNA damage. Scheme 1 provides the synthesis route of MBI-CHO and MBI-CN. The chemical structures were fully characterized through ^{1}H NMR and ^{13}C NMR. The procedures are provided in the supporting information (cf. Electronic Supplementary Material, ESM).

3.1.1 Synthesis of intermediate compound MBI-CHO ((*E*)-4-(2-(1*H*-benzo[*d*]imidazol-2-yl)vinyl) benzaldehyde)

Compound **A** (2-methyl-1*H*-benzo[*d*]imidazole) (1.5 mmol, 200 mg) and terephthalaldehyde (3.0 mmol, 400 mg) were added to the mixed solution of acetic acid and acetic anhydride (1:2, v/v). The resulting solution was stirred and refluxed at 120 °C. The reaction process was monitored through thin-layer chromatography and completed after 4 h. Then, the mixture was cooled to room temperature, and 6.0 mL of concentrated hydrochloric acid was added. The resulting mixture was allowed to stand for 6 h, then poured into water. The solid yellow compound **MBI-CHO** (*E*)-4-(2-(1*H*-benzo[*d*]imidazol-2-yl)vinyl) benzaldehyde was obtained by filtering the solid yellow precipitatt and purifying the crude product through column chromatography on silica gel and eluting the filtered product with dichloromethane/methanol (100:1–10:1, v/v). The yield was 87%. ^{1}H NMR (600 MHz, $(CD_3)_2SO$, δ ppm): 12.86 (s, 1H), 8.54 (s, 1H), 8.02 (d, J = 8.0 Hz, 2H), 7.93 (d, J = 8.0 Hz, 2H), 7.73 (d, J = 16.5 Hz, 1H), 7.58 (s, 2H), 7.46 (d, J = 16.3 Hz, 1H), 7.22 (s, 2H); ^{13}C NMR (151 MHz, $(CD_3)_2SO$, δ ppm): 192.98, 150.82,

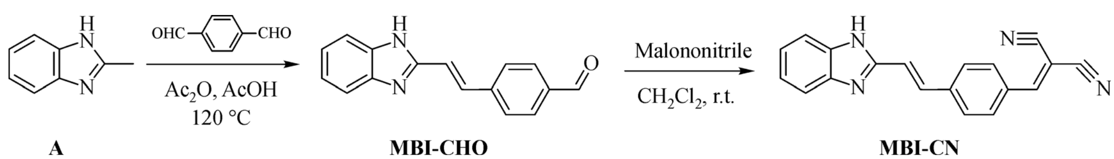

Scheme 1 The synthetic route of compound **MBI-CHO** and **MBI-CN**.

142.08, 136.32, 133.37, 130.60, 128.08, 121.39. HRMS: calculated for $C_{16}H_{12}N_2O$ $[M]^+$ 249.1022, found: 249.1025.

3.1.2 Synthesis of compound MBI-CN ((E)-2-(4-(2-(1H-benzo[d]imidazol-2-yl)vinyl)benzylidene)malononitrile)

Compound **MBI-CHO** (1.2 mmol, 300 mg) and malononitrile (4.0 mmol, 265 mg) were added to the dichloromethane solution. The resulting solution was stirred at room temperature for 4 h. Then, the crude product was obtained, purified, and screened on a silica gel column through column chromatography and eluted with dichloromethane/methanol (50:1–5:1, v/v). The resulting orange solid compound was **MBI-CN** (*E*)-2-(4-(2-(1*H*-benzo[*d*]imidazol-2-yl)vinyl)benzylidene)malononitrile. The yield was 72%. ^{1}H NMR (600 MHz, $(CD_3)_2SO$, δ ppm): 12.80 (s, 1H), 8.53 (s, 1H), 8.02 (d, $J = 8.1$ Hz, 2H), 7.93 (d, $J = 8.2$ Hz, 2H), 7.73 (d, $J = 16.5$ Hz, 1H), 7.57 (s, 2H), 7.46 (d, $J = 16.4$ Hz, 1H), 7.21 (s, 2H); ^{13}C NMR (151 MHz, $(CD_3)_2SO$, δ ppm): 192.98, 150.82, 142.08, 136.32, 133.37, 130.60, 128.08, 121.39. HRMS: calculated for $C_{19}H_{12}N_4$ $[M]^+$ 297.1135, found: 297.1144.

3.2 Optical properties of MBI-CN to mtDNA

The feasibility of designing molecules was verified through spectroscopy. First, the absorption and emission spectra of MBI-CN were obtained in water (Fig. S1, cf. ESM). The result showed that the absorption and emission wavelengths of MBI-CN were at 380 and 620 nm, respectively. MBI-CN was hydrolyzed in a hydrophobic environment. As shown in Fig. 1, with the increase of dimethyl sulfoxide in the aqueous solution (Fig. 1(a)), the emission wavelength of MBI-CN showed blue shifts from 618 nm, and a new emission peak appeared at 483 nm, which belonged to MBI-CHO in the dimethyl sulfoxide solution (Fig. S2, cf. ESM). High-performance liquid chromatography experiments further showed that MBI-CN underwent a hydrolysis reaction and generated MBI-CHO in a hydrophobic environment (Fig. S3, cf. ESM), indicating that MBI-CN was gradually hydrolyzed and it generated MBI-CHO.

The fluorescence intensity of MBI-CN showed no change in water (Fig. S4, cf. ESM), whereas the fluorescence intensity of its intracellular microenvironment-triggering product (i.e., MBI-CHO) decreased at 437 and 553 nm with the increasing mtDNA concentration

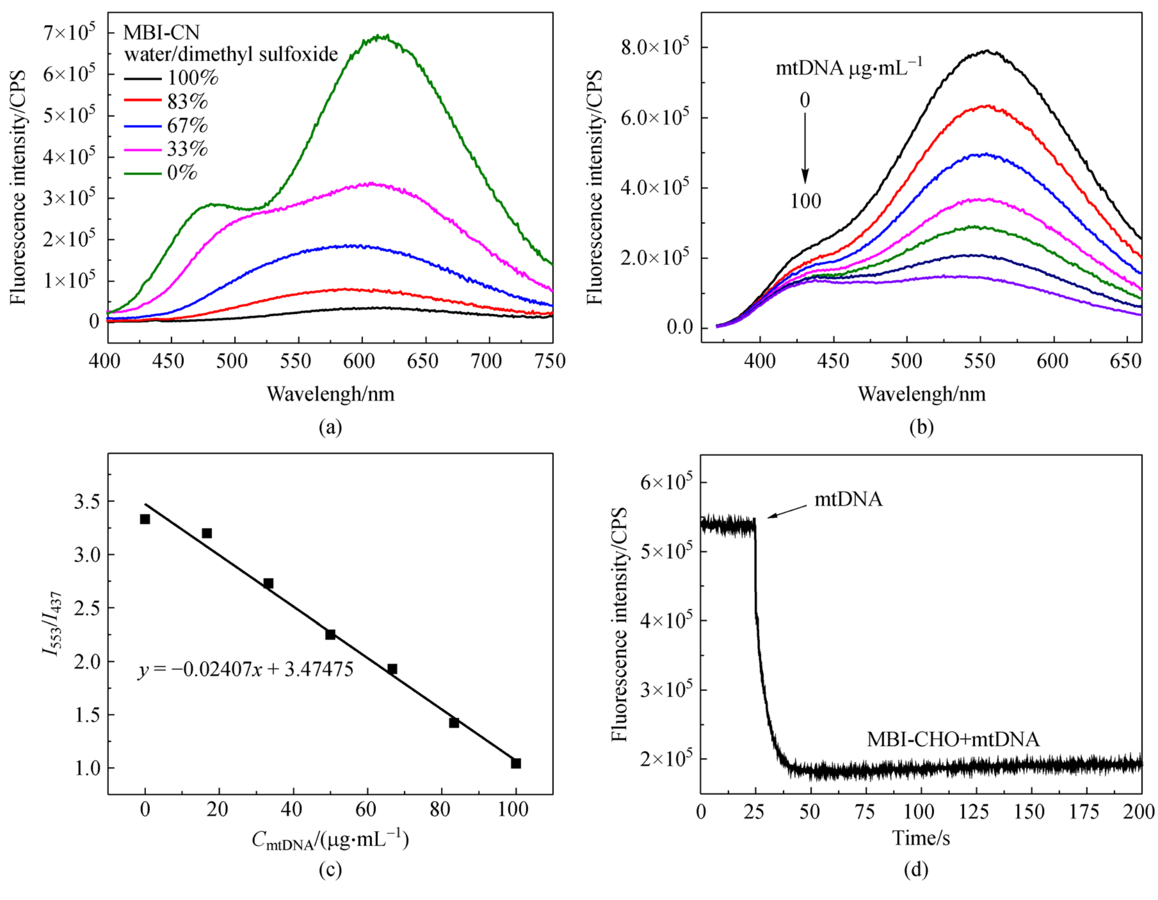

Fig. 1 (a) Fluorescence changes of MBI-CN in different hydrophilic and hydrophobic environments; (b) fluorescence spectrum of MBI-CHO in water with increasing mtDNA concentration (0–100 μg·mL^{-1}); (c) linear relationship diagram between MBI-CHO and mtDNA concentration; (d) MBI-CHO and mtDNA dynamic response.

(Fig. 1(b)). The response for mtDNA showed a good linear relationship, and the detection limit reached 8.17 μg·mL^{-1} (Fig. 1(c)). This result may be attributed to mtDNA damage. The double bond of MBI-CHO can be rotated because of mtDNA damage. The fluorescence intensity of MBI-CHO decreased after it combined with mtDNA. Kinetic experiments showed that MBI-CN underwent a rapid hydrolysis reaction under a hydrophobic action (Fig. S5, cf. ESM) and MBI-CHO can responded to mtDNA within 25 s (Fig. 1(d)). These phenomena indicated that MBI-CN underwent a hydrolysis reaction and generated MBI-CHO in a hydrophobic environment (that is, mtDNA was damaged) and MBI-CHO caused changes in the fluorescence signal for mtDNA damage. Thus, mtDNA damage was detected with MBI-CHO.

3.3 Selectivity of molecules to mtDNA

The intracellular environment is extremely complex, that is, it contains various biological enzymes, ions, and amino acids. For the evaluation of the specific selectivity of MBI-CN and its intracellular microenvironment-triggering product (MBI-CHO), selective tests for related bioactive species were performed (Fig. 2). As shown in Fig. 2(a), MBI-CN and MBI-CHO had no obvious fluorescence responses to bovine serum albumin, hemoglobin, trypsin, lysozyme, amylase, proteinase K, and lipase. The probe did not show any fluorescent response to active small molecules in biological organisms at biologically relevant concentrations (Fig. S6, cf. ESM). By contrast, MBI-CHO as the intracellular microenvironment-triggering product of MBI-CN significantly changed fluorescence intensity after mtDNA damage (Fig. 2(b)). In addition, the probe was stable under physiological conditions (Fig. S7, cf. ESM). These results indicated that MBI-CN can be used in initiating specific response to mtDNA damage in organisms, and the response was not affected by enzymes and small bioactive molecules.

3.4 Mechanism studies

The MBI-CN probe can bind to mtDNA but does not cause spectral chang, which only occurs when MBI-CHO is generated. Therefore, MBI-CHO was used as a supplementary molecule for the detection of experimental results and compared with MBI-CN. In the experiment, the mechanism of interaction of MBI-CN or MBI-CHO with mtDNA was studied. Molecular docking (Fig. 3) showed that MBI-CN and MBI-CHO can be inserted into the large groove of mtDNA and stabilized in mtDNA with hydrogen bonds. The ultraviolet spectrum and circular dichroism were used in further verifying the combination of MBI-CN or MBI-CHO with mtDNA. The ultraviolet spectrum showed (Fig. S8, cf. ESM) that the absorption peak of mtDNA showed a red shift when MBI-CHO was gradually added to mtDNA. This result indicated that the addition of MBI-CHO increased the polarity of mtDNA and weakened the hydrophobic effect [40]. However, when MBI-CN was gradually added to mtDNA, the absorption peak of mtDNA showed a blue shift, indicating that the addition of MBI-CN weakened the polarity of mtDNA and increased the hydrophobic effect [40]. The circular dichroism showed (Fig. 4) that the characteristic peak of mtDNA at 275–280 nm increased [39,41] and the negative peak at 245 nm decreased [41,42] when MBI-CHO and MBI-CN were added to the mtDNA solution. These phenomena indicated that MBI-CN and MBI-CHO can bind to mtDNA in a large groove through hydrogen bond forces [38,43].

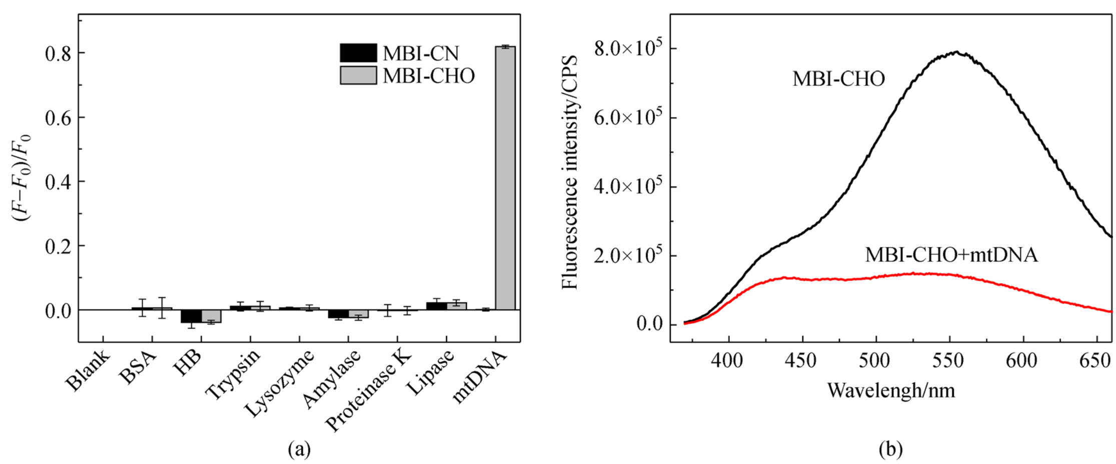

Fig. 2 (a) Fluorescence response of MBI-CN (2 μmol·L^{-1}) and its intracellular microenvironment triggering product MBI-CHO (2 μmol·L^{-1}) to biological enzymes (2 mg·mL^{-1}) (F_0: the initial fluorescence intensity of probes MBI-CN or MBI-CHO; F: the fluorescence intensity after adding interference); (b) Spectra before and after the action of MBI-CHO and MBI-CHO with mtDNA in water.

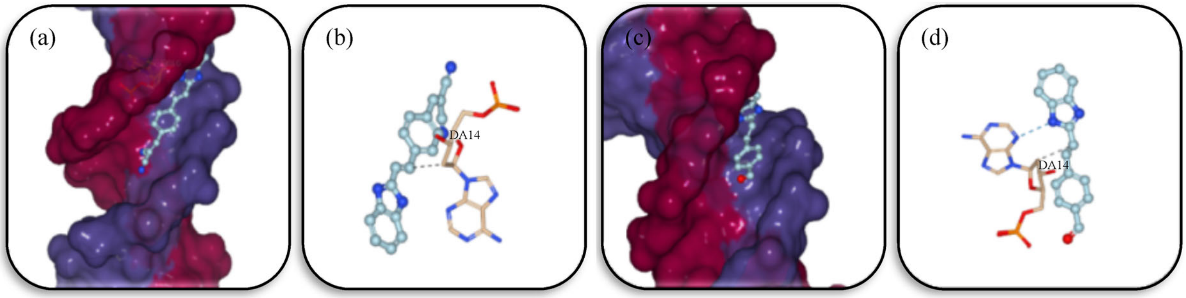

Fig. 3 Results of molecular docking: (a) molecular docking binding mode and (b) binding site of MBI-CN and mtDNA; (c) molecular docking binding mode and (d) binding site of MBI-CHO and mtDNA.

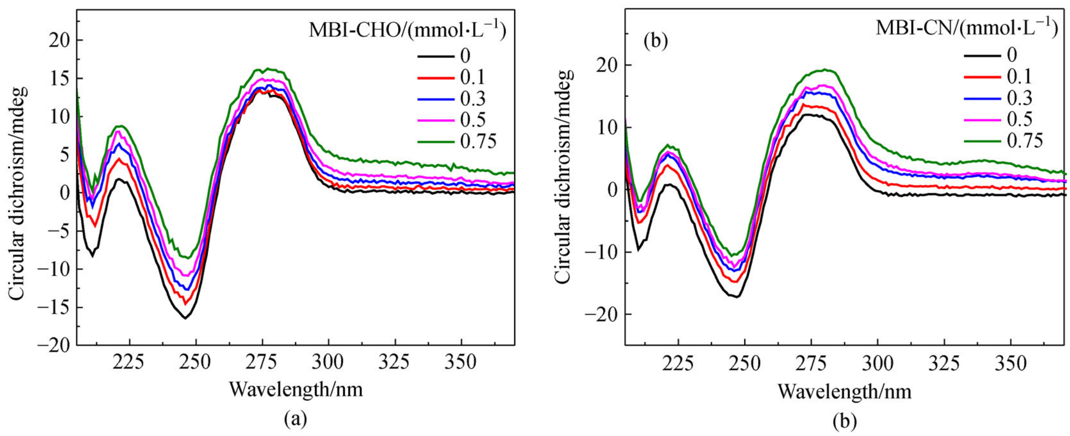

Fig. 4 Circular dichroism analysis of the interaction between molecules and mtDNA: (a) in the Tris-HCl, the concentration of fixed mtDNA (0.25 mg·mL^{-1}) changes with the addition of MBI-CHO to the mtDNA; (b) in the Tris-HCl, the concentration of fixed mtDNA (0.25 mg·mL^{-1}), with the addition of MBI-CN, the optical rotation of mtDNA changes. Cuvette: 1 mm.

3.5 Cytotoxicity experiment

The cytotoxicity of MBI-CN and MBI-CHO was evaluated with the MTT method. As shown in Fig. 5, the cell survival rates of HepG 2 and 3T3 cells remained above 95% after incubation with different concentrations of the probes (5.0, 10.0 and 15.0 μmol·L^{-1}) for 24 h. This result indicated that MBI-CN and MBI-CHO have good biocompatibility.

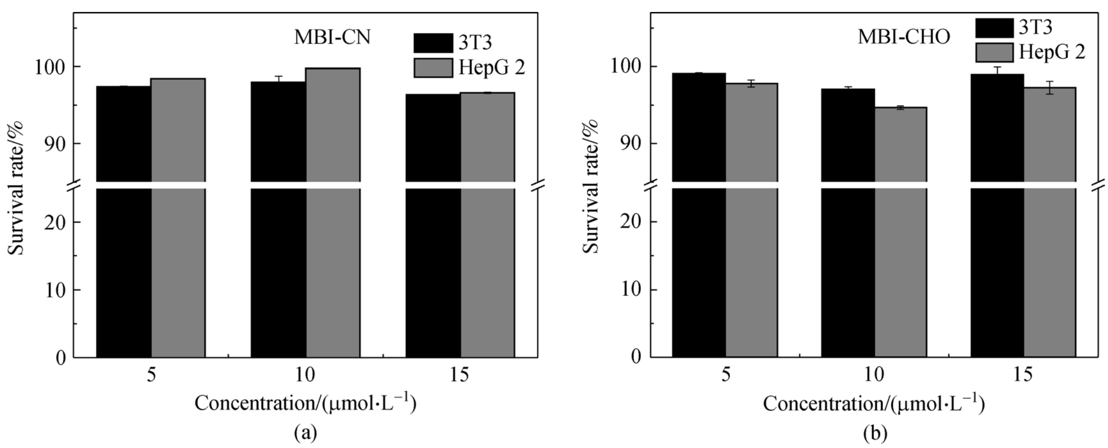

Fig. 5 Cytotoxicity of (a) MBI-CN and (b) MBI-CHO in HepG 2 and 3T3 cells.

3.6 Cell imaging and DNA digestion experiments

This cell imaging experiment verified the imaging capability of the probe in the cells (Fig. 6). Figure 6(b) shows that the probe emitted a bright fluorescent signal at 580–620 nm, and the fluorescent signal presented a regionalized characteristic. Therefore, a cell co-localization experiment was performed to verify the localization of the probe in the cell. The probe was co-cultured with commercial mitochondrial dye (Mito Tracker Green) in the HepG 2 cells. Then, the fluorescence signal of the Mito Tracker Green at 495–535 nm (i.e., the green channel) and the fluorescence signal of MBI-CN at 580–620 nm (i.e., the red channel) were collected. Figure 6(c) shows the Red channel and Mito Tracker Green channels had a good overlap. Pearson's colocalization coefficient (describes the correlation of the intensity distribution between the two channels) was 0.92, showing that MBI-CN can interact with certain substances in the mitochondria.

A cell digestion experiment was performed to further demonstrate that the probe can bind to the mitochondrial DNA (Fig. 7). Figures 7(a,b) show that the Green and Red channels emitted bright fluorescent signals when the cells were not digested. The fluorescence signal of the both channels decreased after digestion by DNA digestibility enzyme in the DNA digestion enzyme digestion model. Figures 7(c,d) show that the Red channel had almost no fluorescence signal after digestion, whereas the Green channel had a weak fluorescence signal. The reason was that mtDNA was destroyed when digested with digestive enzymes. These results indicated that MBI-CN can act on the mitochondria of the cells and bind to mitochondrial DNA.

3.7 Changes caused by mtDNA damage during apoptosis

mtDNA damage is one of the important molecular events in the process of cell apoptosis [44]. The apoptosis model was constructed and used in further verifying the application of the probe. By using catechol as an apoptosis-inducing

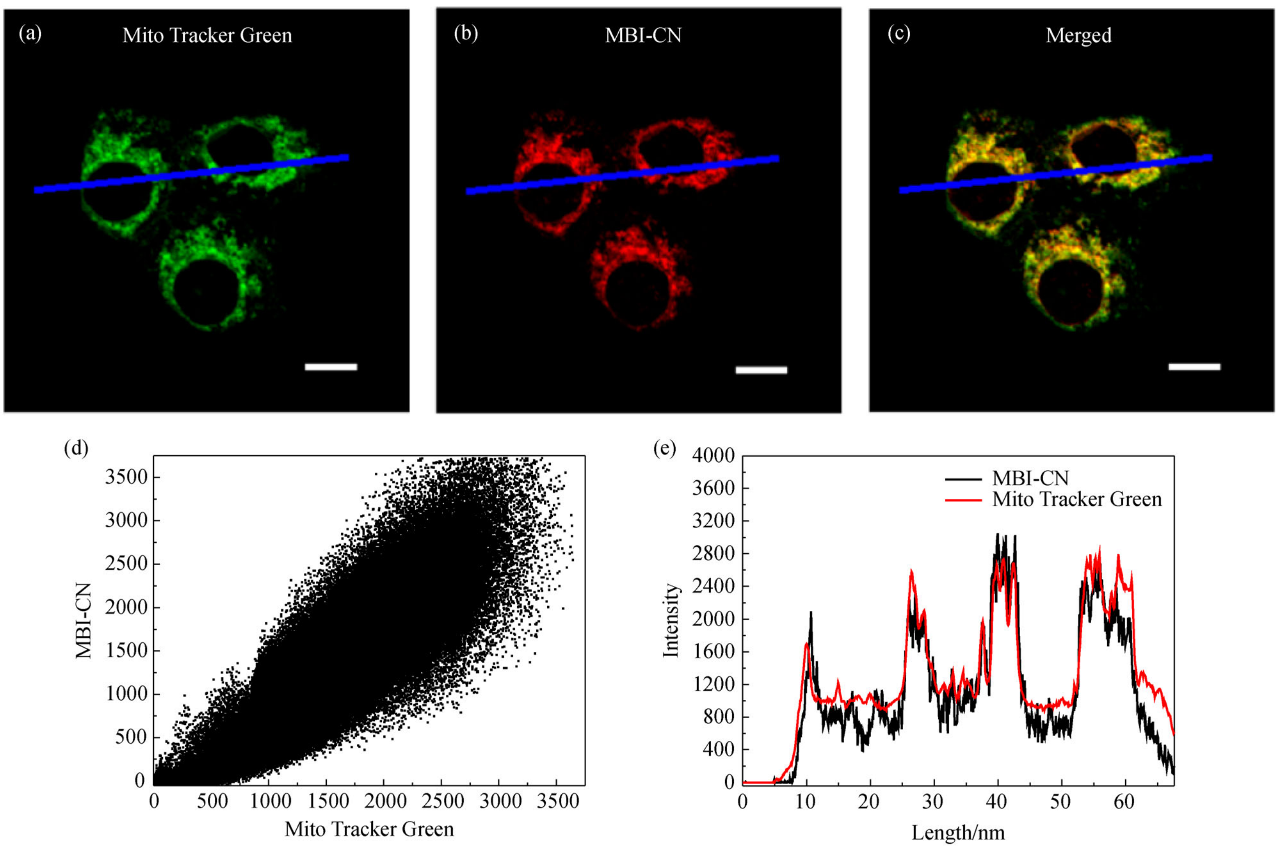

Fig. 6 Cell imaging and cell colocalization experiment: (a) stained with Mito Tracker Green; (b) stained with MBI-CN; (c) merged image of Mito Tracker Green and MBI-CN; (d) intensity correlation plot of stain MBI-CN and Mito Tracker Green; (e) intracellular coregionalization of MBI-CN and Mito Tracker Green. The excitation wavelength of MBI-CN is 405 nm and the fluorescence collection range is 580–620 nm; the excitation wavelength of Mito Tracker Green is 488 nm and the fluorescence collection range is 495–535 nm. The scale bar represents 10 μm.

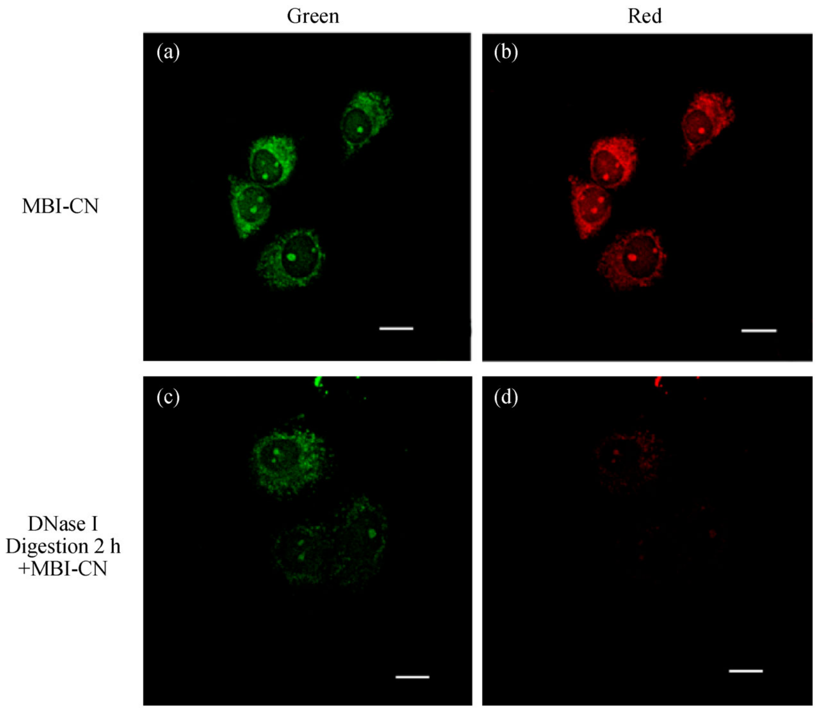

Fig. 7 DNA digestion experiments: after fixing cells, MBI-CN cell imaging in (a) green and (b) red channel; after digestion with DNA digestion enzyme for 2.0 h, added MBI-CN and incubated for 30 min, MBI-CN cell imaging in (c) green and (d) red channel. The excitation wavelength is 405 nm, and the fluorescence collection ranges are 415–465 nm (Green channel) and 530–570 nm (Red channel). Scale bar: 10 μm.

factor, an apoptosis model was constructed in HepG 2 cells [45]. After 24 h, different concentrations (0, 0.2 and 1.0 mmol·L^{-1}) of catechol were added and incubated with the cells for 36 h. Then, the probe (7.5 μmol·L^{-1}) was added to a Petri dish and incubated for 30 min for imaging (Fig. 8). The experimental results showed that the untreated cells showed bright fluorescent signals in the Green channel (Fig. 8(a)) and Red channel (Fig. 8(d)). After induction with different concentrations of catechol, the fluorescence signals of the two channels gradually decreased with increasing degree of apoptosis, and the Green channel decreased (Figs. 8(b,c)) to a lower degree than the Red channel (Figs. 8(e,f)). The experimental results showed that mtDNA was damaged during cell apoptosis, and the degree of damage was evaluated according to the changes in probe fluorescence. This result was consistent with the results of *in vitro* spectroscopy experiments. These results indicated that MBI-CN can be used as a new detection tool for the rapid and specific monitoring of mtDNA damage in cells.

4 Conclusions

A reactive probe was designed and developed for the monitoring and evaluation of the degree of mtDNA damage. The probe was triggered by the hydrophobic environment of mtDNA damage *in situ*. In the molecular design, the hydrolytic rate-limiting reaction of malononitrile was selected as the specific recognition reaction. Given that the molecule needs to enter the mtDNA double strand and cannot cause additional damage to mtDNA, a typical dye molecule was selected, namely MBI, as a fluorophore. In a hydrophobic environment, MBI-CN was constructed by using malononitrile to initiate the hydrolysis reaction in a hydrophobic environment. It effectively prevented interferences to the detection of organism self-fluorescence and accurately reflected the degree of mtDNA damage. MBI-CHO, as the product of MBI-CN, showed weak fluorescence at 437 and 553 nm when mtDNA damage occurred within 25 s. These results showed that the probe can respond to mtDNA damage rapidly and specifically. Furthermore, MBI-CN and MBI-CHO showed good biocompatibility, indicating that the probe can achieve the above-mentioned rapid detection process without causing additional mtDNA damage. Thus, MBI-CN was successfully used in monitoring mtDNA damage during apoptosis, and the degree of mtDNA damage was preliminarily evaluated. Hence, MBI-CN can be used as an effective monitoring tool for quickly and specifically monitoring and evaluating mtDNA damage in a variety of biological processes.

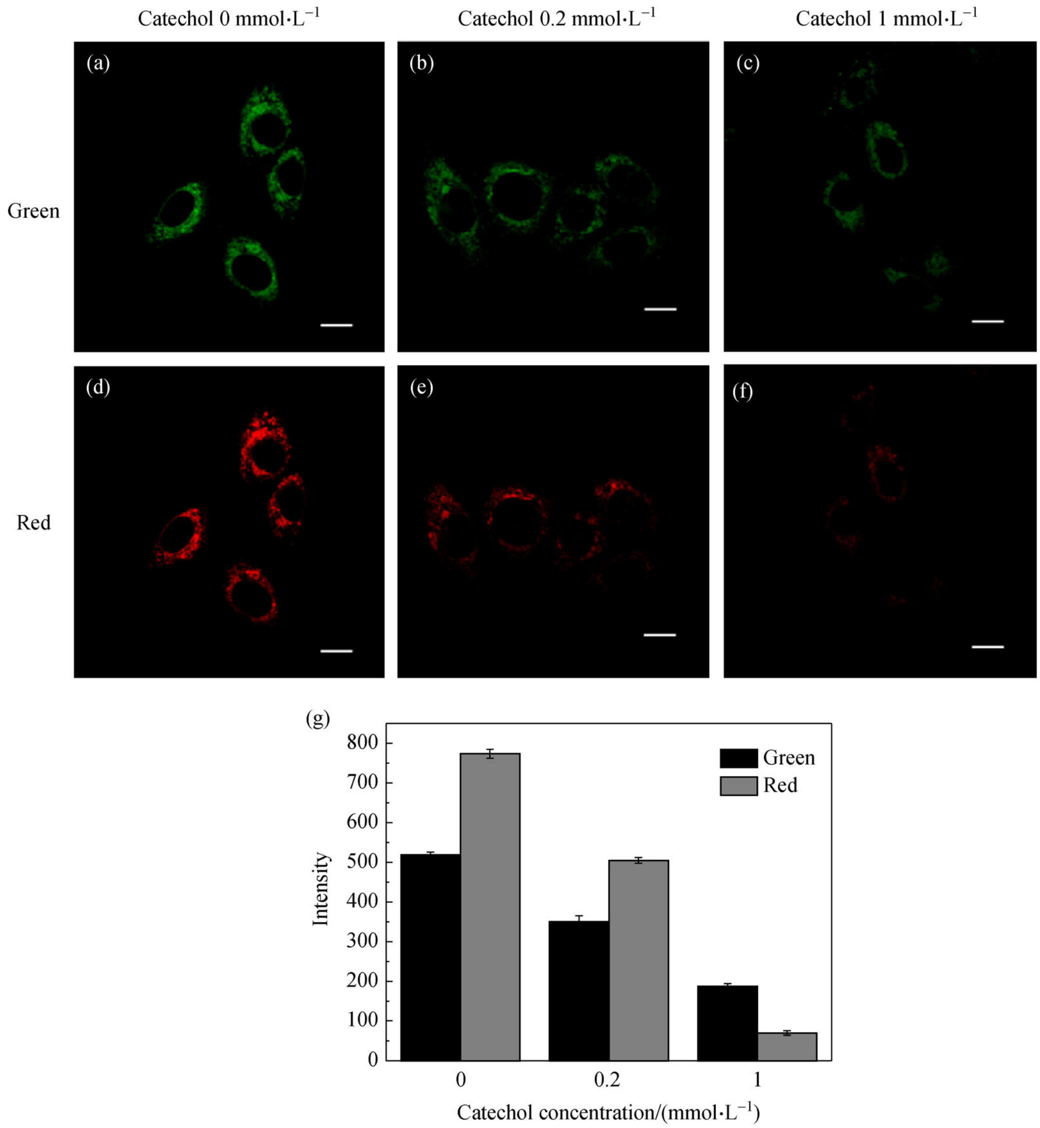

Fig. 8 Apoptosis experiment: cell apoptosis was induced by different concentrations of catechol, and then MBI-CN (7.5 μmol·L^{-1}) was added for 30 min. (a,d) Concentrations of catechol: 0 mmol·L^{-1}; (b,e) concentrations of catechol: 0.2 mmol·L^{-1}; (c,f) concentrations of catechol: 1.0 mmol·L^{-1}; (g) apoptosis imaging fluorescence intensity extraction image. The excitation wavelength is 405 nm, and the fluorescence collection ranges are 415–465 nm (Green channel) and 530–570 nm (Red channel). Scale bar: 10 μm.

Acknowledgements This work was supported by the National Natural Science Foundation of China (Grant Nos. 21722501 and 22004028), Henan Special Support for High-level Talents Central Plains Science and Technology Innovation Leading Talents (Grant No. 204200510006), Key Project of Science and Technology of Henan Province (Grant No. 202102310139).

Electronic Supplementary Material Supplementary material is available in the online version of this article at https://dx.doi.org/10.1007/s11705-021-2063-9 and is accessible for authorized users.

References

1. Kuchlyan J, Martinez-Fernandez L, Mori M, Gavvala K, Ciaco S, Boudier C, Richert C, Didier P, Tor Y, Improta R, Mély Y. What makes thienoguanosine an outstanding fluorescent DNA probe. Journal of the American Chemical Society, 2020, 142(40): 16999–17014
2. Gao F L, Li L J, Fan J L, Cao J F, Li Y Q, Chen L Y, Peng X J. An off-on two-photon carbazole-based fluorescent probe: highly targeting and super-resolution imaging of mtDNA. Analytical Chemistry, 2019, 91(5): 3336–3341
3. Yakes F M, Van Houten B. Mitochondrial DNA damage is more extensive and persists longer than nuclear DNA damage in human cells following oxidative stress. Proceedings of the National Academy of Sciences of the United States of America, 1997, 94 (2): 514–519
4. Vladimir B S, Evgeny E, Natalia A, Maria A A, Sergey I N, Georgii A B, Igor A, Shamil R S. Error-prone bypass of DNA lesions during

lagging-strand replication is a common source of germline and cancer mutations. Nature Genetics, 2019, 51(1): 36–41
5. Anderson S, Bankier A T, Barrell B G, De Bruijn M H, Coulson A R, Drouin J, Eperon I C, Nierlich D P, Roe B A, Sanger F, Schreier P H, Smith A J H, Staden R, Young I G. Sequence and organization of the human mitochondrial genome. Nature, 1981, 290(5806): 457–465
6. Bibb M J, Van Etten R A, Wright C T, Walberg M W, Clayton D A. Sequence and gene organization of mouse mitochondrial DNA. Cell, 1981, 26(2): 167–180
7. Assaf C B, Maayan R, Yifat S O, Michael M I, Dan S, Malka C, Aaron B, Gideon Z, Donna S S, Batsheva K. Nucleotide deficiency promotes genomic instability in early stages of cancer development. Cell, 2011, 145(3): 435–446
8. Makoto R H, Jeffrey J K, Erin J W, Sudarshan R, Ryan T S, Wayne G, Aaron J T, Barbara W, Christopher M L, Kunhong X, et al. A stress response pathway regulates DNA damage through β2-adrenoreceptors and β-arrestin-1. Nature, 2011, 477(7364): 349–353
9. Furda A M, Marrangoni A M, Lokshin A, Van Houten B. Oxidants and not alkylating agents induce rapid mtDNA loss and mitochondrial dysfunction. DNA Repair, 2012, 11(8): 684–692
10. Feng B D, Wang K, Liu J W, Mao G J, Cui J Q, Xuan X P, Jiang K, Zhang H. Ultrasensitive apurinic/apyrimidinic site-specific ratio fluorescent rotor for real-time highly selective evaluation of mtDNA oxidative damage in living cells. Analytical Chemistry, 2019, 91 (21): 13962–13969
11. Neiman M, Taylor D R. The causes of mutation accumulation in mitochondrial genomes. Proceedings. Biological Sciences, 2009, 276(1660): 1201–1209
12. Furda A M, Marrangoni A M, Lokshin A, Van Houten B. Oxidants and not alkylating agents induce rapid mtDNA loss and mitochondrial dysfunction. DNA Repair, 2012, 11(8): 684–692
13. Schon E A, DiMauro S, Hirano M. Human mitochondrial DNA: roles of inherited and somatic mutations. Nature Reviews. Genetics, 2012, 13(12): 878–890
14. Schuermann D, Scheidegger S P, Weber A R, Bjoras M, Leumann C J, Schar P. 3CAPS—a structural AP-site analogue as a tool to investigate DNA base excision repair. Nucleic Acids Research, 2016, 44(5): 2187–2198
15. Bender A, Krishnan K J, Morris C M, Taylor G A, Reeve A K, Perry R H, Jaros E, Hersheson J S, Betts J, Klopstock T, Taylor R W, Turnbull D M. High levels of mitochondrial DNA deletions in substantia nigra neurons in aging and parkinson disease. Nature Genetics, 2006, 38(5): 515–517
16. Rebbeck C A, Leroi A M, Burt A. Mitochondrial capture by a transmissible cancer. Science, 2011, 331(6015): 303
17. Ascaso F J, Lopez-Gallardo E, DelPrado E, Ruiz-Pesini E, Montoya J. Macular lesion resembling adult-onset vitelliform macular dystrophy in Kearns-Sayre syndrome with multiple mtDNA deletions. Clinical & Experimental Ophthalmology, 2010, 38(8): 812–816
18. Badura-Stronka M, Wawrocka A, Zawieja K, Silska S, Krawczynski M R. Severe manifestation of Leber's hereditary optic neuropathy due to 11778G > A mtDNA mutation in a female with hypoestrogenism due to perrault syndrome. Mitochondrion, 2013, 13(6): 831–834
19. Sun W, Li M, Fan J L, Peng X J. Activity-based sensing and theranostic probes based on photoinduced electron transfer. Accounts of Chemical Research, 2019, 52(10): 2818–2831
20. Sun W, Guo S G, Hu C, Fan J L, Peng X J. Recent development of chemosensors based on cyanine platforms. Chemical Reviews, 2016, 116(14): 7768–7817
21. Lin F, Zhou Y F, Li Q S, Zhou X S, Shao Y, Haber-meyer B, Wang H, Shi X H, Xu Z A. Prototropically allosteric probe for superbly selective DNA analysis. Analytical Chemistry, 2017, 89(17): 9299–9306
22. Zou X X, Shi Y L, Zhu R, Han J H, Han S F. Organelle-redirected chameleon sensor-enabled live cell imaging of mitochondrial DNA. Analytical Chemistry, 2019, 91(24): 15899–15907
23. Abeywickrama C S, Bertman K A, Plescia C B, Stahelin R V, Pang Y. Structural effect on the cellular selectivity of an NIR-emitting cyanine probe: from lysosome to simultaneous nucleus and mitochondria selectivity with potential for monitoring mitochondria dysfunction in cells. ACS Applied Bio Materials, 2019, 2(11): 5174–5181
24. Briggs C, Jones M. SYBR Green I-induced fluorescence in cultured immune cells: a comparison with acridine orange. Acta Histochemica, 2005, 107(4): 301–312
25. Davis S K, Bardeen C J. Cross-linking of histone proteins to DNA by UV illumination of chromatin stained with hoechst 33342. Photochemistry and Photobiology, 2003, 77(6): 675–679
26. Pfeifer G P, You Y H, Besaratinia A. Mutations induced by ultraviolet light. Mutation Research, 2005, 571(1-2): 19–31
27. Smith P J, Blunt N, Wiltshire M, Hoy T, Teesdale-Spittle P, Craven M R, Watson J V, Amos W B, Errington R J, Patterson L H. Characteristics of a novel deep red/infrared fluorescent cell-permeant DNA probe, DRAQ5, in intact human cells analyzed by flow cytometry, confocal and multiphoton microscopy. Cytometry, 2000, 40(4): 280–291
28. Burke C S, Byrne A, Keyes T E. Highly selective mitochondrial targeting by a ruthenium(II) peptide conjugate: imaging and photoinduced damage of mitochondrial DNA. Angewandte Chemie International Edition, 2018, 57(38): 12420–12424
29. Cao J J, Zheng Y, Wu X W, Tan C P, Chen M H, Wu N, Ji L N, Mao Z W. Anticancer cyclometalated iridium(III) complexes with planar ligands: mitochondrial DNA damage and metabolism disturbance. Journal of Medicinal Chemistry, 2019, 62(7): 3311–3322
30. Zheng Y, Zhang D Y, Zhang H, Cao J J, Tan C P, Ji L N, Mao Z W. Photodamaging of mitochondrial DNA to overcome cisplatin resistance by a Ru II–Pt II bimetallic complex. Chemistry (Weinheim an der Bergstrasse, Germany), 2018, 24(71): 18971–18980
31. Feng B D, Wang K, Yang Y G, Wang G, Zhang H, Liu Y F, Jiang K. Ultrasensitive recognition of AP sites in DNA at the single-cell level: one molecular rotor sequentially self-regulated to form multiple different stable conformations. Chemical Science (Cambridge), 2019, 10(44): 10373–10380
32. Peng X J, Wu T, Fan J L, Wang J Y, Zhang S, Song F L, Sun S G. An effective minor groove binder as a red fluorescent marker for live-cell DNA imaging and quantification. Angewandte Chemie International Edition, 2011, 50(18): 4180–4183

33. Friedberg E C. DNA damage and repair. Nature, 2003, 421(6921): 436–440
34. Song Y L, Tian T, Shi Y Z, Liu W L, Zou Y, Khajvand T, Wang S L, Zhu Z, Yang C Y. Enrichment and single-cell analysis of circulating tumor cells. Chemical Science (Cambridge), 2017, 8(3): 1736–1751
35. Leung C H, Zhong H J, He H Z, Lu L, Chan D S H, Ma D L. Luminescent oligonucleotide-based detection of enzymes involved with DNA repair. Chemical Science (Cambridge), 2013, 4(10): 3781–3795
36. Liu C X, Wang Y F, Zhang X, Wu F, Yang W, Zou G G, Yao Q, Wang J Q, Chen Y Q, Wang S R, Zhou X. Enrichment and fluorogenic labelling of 5-formyluracil in DNA. Chemical Science (Cambridge), 2017, 8(6): 4505–4510
37. Visvardis E E, Tassiou A M, Piperakis S M. Study of DNA damage induction and repair capacity of fresh and cryopreserved lymphocytes exposed to H_2O_2 and γ-irradiation with the alkaline comet assay. Mutation Research, 1997, 383(1): 71–80
38. Berova N, Nakanishi K, Woody R W. Circular Dichroism: Principles and Applications. New York: Wiley-VCH, 2000, 703–718
39. Monnot M, Mauffret O, Lescot E, Fermandjian S. Probing intercalation and conformational effects of the anticancer drug 2-methyl-9-hydroxyellipticinium acetate in DNA fragments with circular dichroism. European Journal of Biochemistry, 1992, 204 (3): 1035–1039
40. Karami K, Shirani-Sarmazeh Z, Hosseini-Kharat M, Lipkowski J, Saeidifar M. Synthesis, spectral characterization, crystal structure and *in vitro* DNA/protein binding studies of phosphorous ylide palladacyclic complexes containing azide group. Journal of Photochemistry and Photobiology. B, Biology, 2015, 144: 11–19
41. Baase W A, Johnson W C Jr. Circular dichroism and DNA secondary structure. Nucleic Acids Research, 1979, 6(2): 797–814
42. Sarkar D, Das P, Basak S, Chattopadhyay N. Binding interaction of cationic phenazinium dyes with calf thymus DNA: a comparative study. Journal of Physical Chemistry B, 2008, 112(30): 9243–9249
43. Poulsen B C, Estalayo-Adrián S, Blasco S, Bright S A, Kelly J M, Williams D C, Gunnlaugsson T. Luminescent ruthenium polypyridyl complexes with extended 'dppz' like ligands as DNA targeting binders and cellular agents. Dalton Transactions (Cambridge, England), 2016, 45(45): 18208–18220
44. Fishel M L, Seo Y R, Smith M L, Kelley M R. Imbalancing the DNA base excision repair pathway in the mitochondria; targeting and overexpressing *N*-methylpurine DNA glyeosylase in mitochondria leads to enhanced cell killing. Cancer Research, 2003, 63(3): 608–615
45. Scaduto R C Jr, Grotyohann L W. Measurement of mitochondrial membrane potential using fluorescent rhodamine derivatives. Biophysical Journal, 1999, 76(1): 469–477